A Composite Ansatz for Calculation of Dynamical Structure Factor

Yupei Zhang(张玉佩)[1], Chongjie Mo(莫崇杰)[2*], Ping Zhang(张平)[3,4], and Wei Kang(康炜)[4*]

[1]*HEDPS, Center for Applied Physics and Technology, and School of Physics, Peking University, Beijing 100871, China*
[2]*Beijing Computational Science Research Center, Beijing 100193, China*
[3]*Institute of Applied Physics and Computational Mathematics, Beijing 100088, China*
[4]*HEDPS, Center for Applied Physics and Technology, and College of Engineering, Peking University, Beijing 100871, China*

(Received 27 November 2023; accepted manuscript online 19 December 2023)

We propose an ansatz without adjustable parameters for the calculation of a dynamical structure factor. The ansatz combines the quasi-particle Green's function, especially the contribution from the renormalization factor, and the exchange-correlation kernel from time-dependent density functional theory together, verified for typical metals and semiconductors from a plasmon excitation regime to the Compton scattering regime. It has the capability to reconcile both small-angle and large-angle inelastic x-ray scattering (IXS) signals with much-improved accuracy, which can be used as the theoretical base model, in inversely inferring electronic structures of condensed matter from IXS experimental signals directly. It may also be used to diagnose thermal parameters, such as temperature and density, of dense plasmas in x-ray Thomson scattering experiments.

DOI: 10.1088/0256-307X/41/1/017801

Dynamical structure factor (DSF) $S(\boldsymbol{q}, \omega)$ is a straight-forward description for the correlated motion of electrons in solids[1–3] and dense plasmas,[4–7] and whereby of persisting interests in a variety of research branches.[8–15] Since it can be directly detected in inelastic x-ray scattering (IXS) experiments[2,16–20] or electron energy loss experiments[21–23] with a resolution on both transferred momentum $\boldsymbol{q}$ and frequency ω, DSF has been long considered as a prospective tool to infer electronic structures and collective excitations in a many-electron system. In condensed materials, a number of properties associated with electronic structures and excitations, e.g., plasmon excitation,[3,18,24,25] double-plasmon excitation,[3,26–29] near-edge structures,[30–34] single-particle excitation continuum,[35] and even part of excitonic effect,[36,37] are considered to present in the DSF with detectable features. In dense plasmas, DSF, usually probed in x-ray Thomson scattering experiments, is considered as an important, and sometimes irreplaceable, diagnostic tool to probe thermal properties, such as temperature and density, in the internal regime of dense plasmas.[5,38–42]

It is a common practice to calculate DSF in the framework of time-dependent density functional theory (TDDFT),[43,44] which avoids the cumbersome calculation of the Bethe–Salpeter equation[1,45] of the many-body perturbation theory (MBPT) approach, owing to the less important contribution of long-range exchange and correlation effect in the DSF.[1] It was shown[16,25,35,46,47] as a rule of the thumb that for $|\boldsymbol{q}|$ smaller than twice of the plasmon cutoff wave vector q_c, the method reproduced the experimental DSF well with lifetime broadening effects included semi-empirically. Beyond that, theoretical results significantly differ from experimental measurements. Thus having a theoretical approach that is able to reconcile DSF to much larger $|\boldsymbol{q}|$ has been longed for, so that large-angle x-ray scattering signal may also be well interpreted. If so, the capability of various light sources, including synchrotron light sources[10,12–16,18,24,28,31,33,36] and the free-electron laser light sources,[6,48,49] would be much strengthened.

In this Letter, we propose an ansatz with no adjustable parameter to reconcile DSF measurements, verified for valence electrons of metals and semiconductors (including lithium, sodium, aluminum, and silicon) from the plasmon excitation regime to the Compton scattering regime. The ansatz contains two major ingredients: the contributions of the quasi-particle Green's function, including those from quasi-particle energy-level shifts, lifetime broadening, and renormalization factors;[50–52] together with the corrections from the TDDFT kernel, which contributes to the effective local field effect.[16,25,35,46] We show that the contributions of the quasi-particle Green's function and of the TDDFT kernel, though originated from distinct theoretical frameworks (i.e., from MBPT and TDDFT respectively), can be combined together to arrive at a simple but effective formula.

Formally, $S(\boldsymbol{q}, \omega)$ can be derived from the response function $\chi(\boldsymbol{q}, \boldsymbol{q}', \omega)$ through the fluctuation-dissipation theorem,[53] i.e., $S(\boldsymbol{q}, \omega) = -\Im[\chi(\boldsymbol{q}, \boldsymbol{q}', \omega)]|_{\boldsymbol{q}'=\boldsymbol{q}}/(\pi n)$,

*Corresponding authors. Email: cjmo@csrc.ac.cn; weikang@pku.edu.cn
© 2024 Chinese Physical Society and IOP Publishing Ltd

where n is the electronic density. The screening effect is accounted for by a Dyson-like equation [44]

$$\chi(\boldsymbol{q}, \boldsymbol{q}', \omega) = \chi_0(\boldsymbol{q}, \boldsymbol{q}', \omega) + \int d\boldsymbol{q}_1 d\boldsymbol{q}_2 \chi_0(\boldsymbol{q}, \boldsymbol{q}_1, \omega) \cdot K(\boldsymbol{q}_1, \boldsymbol{q}_2, \omega)\chi(\boldsymbol{q}_2, \boldsymbol{q}', \omega), \quad (1)$$

where $\chi_0(\boldsymbol{q}, \boldsymbol{q}', \omega)$ is the bare response function, and $K(\boldsymbol{q}, \boldsymbol{q}', \omega)$ is the many-body interaction kernel.

In the ansatz, χ_0 and K are treated separately. The kernel $K(\boldsymbol{q}, \boldsymbol{q}', \omega)$ is approximated as the sum of Coulomb contribution $v_c(q) = 4\pi/|\boldsymbol{q}|^2$ and an effective contribution containing exchange and correlation effects $f_{xc}(\boldsymbol{q}, \boldsymbol{q}', \omega)$ from TDDFT, i.e.,

$$K(\boldsymbol{q}, \boldsymbol{q}', \omega) = v_c(q)\delta(\boldsymbol{q} - \boldsymbol{q}') + f_{xc}(\boldsymbol{q}, \boldsymbol{q}', \omega). \quad (2)$$

Equations (1) and (2) will be reduced to the random phase approximation of χ when f_{xc} is set to be zero.

The bare response function $\chi_0(\boldsymbol{q}, \boldsymbol{q}', \omega)$ is calculated as the Fourier transform of $\chi_0(\boldsymbol{r}, t; \boldsymbol{r}', t')$, where $\boldsymbol{r}$ and $\boldsymbol{r}'$ are coordinates in the three-dimensional space, and

$$\chi_0(\boldsymbol{r}, t; \boldsymbol{r}', t') = -iG(\boldsymbol{r}, t; \boldsymbol{r}', t')G(\boldsymbol{r}', t'; \boldsymbol{r}, t)/\zeta. \quad (3)$$

Here, $G(\boldsymbol{r}, t; \boldsymbol{r}', t')$ is the screened Green's function, and ζ is an amplitude scaling constant to numerically guarantee the sum rule $\int_{-\infty}^{\infty} \omega S(\boldsymbol{q}, \omega)d\omega = |\boldsymbol{q}|^2/2$ (atomic units). [54] With the help of a set of quasi-particle wave functions, denoted as $\phi_j(\boldsymbol{r})$ with j the index of wave functions, $\chi_0(\boldsymbol{r}, \boldsymbol{r}'; \omega)$ can be recast as

$$\chi_0(\boldsymbol{r}, \boldsymbol{r}'; \omega) = \sum_{j \neq k} (f_j - f_k) \frac{|Z_k||Z_j|}{\zeta} \cdot \frac{\phi_k(\boldsymbol{r})\phi_j^*(\boldsymbol{r})\phi_j(\boldsymbol{r}')\phi_k^*(\boldsymbol{r}')}{\omega - (\epsilon_k^{QP} - \epsilon_j^{QP})}, \quad (4)$$

where ϵ_j^{QP} and Z_j are quasi-particle energy and renormalization factor associated with the j-th quasi-particle state, and f_j is the effective occupation number; ζ is then determined as the product of the renormalization factors of the highest quasi-holes (denoted as Z^-) and of the lowest quasi-electrons (denoted as Z^+) with respect to the Fermi level, i.e., $\zeta = |Z^+Z^-|$. It is crucial in the ansatz to set ζ in this particular form, which not only recovers the sum rule, but also accounts for the significant improvements in the DSF spectra at high transferred momenta.

In practice, the quasi-particle properties are calculated using the GW method. [50,51,55] In particular, we follow Ref. [51] for the calculation of ϵ_j^{QP}, Z_j, and $\phi_j(\boldsymbol{r})$, which means that $\phi_j(\boldsymbol{r})$ is approximated by the corresponding Kohn–Sham wave function $\phi_j^{KS}(\boldsymbol{r})$, $\epsilon_j^{QP} = \epsilon_j^{KS} + Z_j\langle\phi_j|\Sigma(\epsilon_j^{KS}) - V_{xc}^{KS}|\phi_j\rangle$, and $Z_j^{-1} = 1 - \frac{\partial\Sigma_j(\omega)}{\partial\omega}|_{\omega=\epsilon_j^{KS}}$. Here, Σ is the self-energy operator, ϵ_j^{KS} is the Kohn–Sham eigen-energy associated with ϕ_j^{KS}, and V_{xc}^{KS} is the exchange-correlation potential. Note that now both Z_j and ϵ_j^{QP} are complex numbers, and the imaginary parts of ϵ_j^{QP} for quasi-holes and quasi-electrons have opposite signs. So, Eq. (4) naturally contains a damping coefficient $\eta = \Im(\epsilon_k^{QP} - \epsilon_j^{QP}) = |\Im\Sigma_k| + |\Im\Sigma_j|$. [16,25,35,46]

Here, we take lithium (Li) and silicon (Si) crystalline structures as demonstrating examples to display the performance of the new method, where Li is a typical metal and Si is considered as a prototype of semiconductors. In the calculations, the lattice constant is set to be 6.6 bohr for Li and 10.26 bohr for Si, taken from measured values at room temperature. [56–59] Kohn–Sham eigen-energies ϵ_j^{KS} and corresponding wave functions ϕ_j^{KS} are obtained from a ground-state density functional theory (DFT) calculation via the `Quantum Espresso` package, [60,61] using norm-conserving pseudopotentials with only valence electrons included, i.e., one $2s$ electron for Li and four $3s3p$ electrons for Si. The cutoff radii of the pseudopotentials are 2.97 bohr for Li and 1.8 bohr for Si, which yields convergent results at a plane wave cutoff energy of 80 Ry for both Li and Si, as have been carefully examined. In order to have a close comparison with preceding results, [16,46] a local density approximation version of exchange-correlation functional is used. To match the transferred momentum $\boldsymbol{q}$ in experimental measurements, a much-refined Monkhorst–Pack $\boldsymbol{k}$-point mesh [62] is adopted. It varies from $8 \times 8 \times 8$ to $14 \times 14 \times 14$ so that one can find a $\boldsymbol{q}$ in the calculation, which is close to the experimental transferred momentum with a difference less than 3%.

All DSF calculations, including calculations of quasi-particle properties using the GW method, are carried out using the `Yambo` code. [63,64] Here, a necessary revision is carried out by introducing the rescaling coefficient $\Gamma = |Z_k||Z_j|/\zeta$ into the calculation of the bare response function via Eq. (4) in order to reasonably deal with the effect of the renormalization factor. In the GW calculations, the screening cutoff is 10 Ry, and the self-energy cutoff is 15 Ry with 240 bands included. When χ is calculated via Eqs. (1) and (2), the adiabatic local density approximation (ALDA) [65] for f_{xc} is adopted. A more sophisticated form of f_{xc} is also possible, but turns out to have a small effect on metallic and typical semiconductor materials. The DSF spectra presented are further smoothed with a Gaussian smearing γ varying from 0.5 to 2.5 eV following Ref. [39] to account for the finite resolution in ω caused by the discrete sampling of the Brillouin zone. The smearing increases with $|\boldsymbol{q}|$, and is explicitly indicated in each calculation.

Figure 1 shows the calculated DSF of Li, along the [100] and [111] directions. The transferred momenta vary from 0.28 to 1.40 bohr^{-1}. In the figure, the results of the new method are displayed as ALDA+G and red solid curves, meaning that all features of Green's function are included in conjunction with an ALDA f_{xc} in Eq. (2). The results of the original TDDFT method are displayed as ALDA and blue dotted curves, and those calculated with ALDA f_{xc} and lifetime corrections, as proposed in Refs. [25,35], are denoted as ALDA+LT together with green dashed curves. For comparison purposes, IXS measurements [2,18,19] are also presented in the figure, as displayed by solid scattering dots.

Figure 1(a) shows the capability of the new method to capture the feature of plasmon peak at small but finite $|\boldsymbol{q}|$, which is located around 7 eV. It shows that the new

calculation closely follows the experimental data. In this regime, it has also been known in practice that the TDDFT method with the ALDA kernel reproduces the experimental spectrum well for metals, as displayed by the dotted curve.

Figure 1(b) illustrates the necessity of lifetime broadening in metallic systems, where $|\boldsymbol{q}|$ is between q_c and $2q_c$. Note that q_c for Li is about 0.46 bohr^{-1}.[2] An important feature of the spectrum is the narrow shoulder at about 12 eV, as indicated by the arrow. Without lifetime effects, the ALDA calculation presents a separate small peak, which is clearly different from the narrow-shoulder feature of the experimental spectrum (displayed as scattering points). This deviation can be remedied by including the lifetime broadening effect, i.e., the imaginary part of quasi-particle energies, as has been pointed out in the work of Weissker *et al.*[16,46] The figure shows that both the new ALDA+G and ALDA+LT methods, which take the lifetime broadening into consideration, indeed smooth out the peak and give a much closer agreement to the experimental spectrum. It also shows that other quasi-particle features in the new method, such as the quasi-particle energy shift and the renormalization factor, do not contribute significant corrections to the spectrum at this $|\boldsymbol{q}|$.

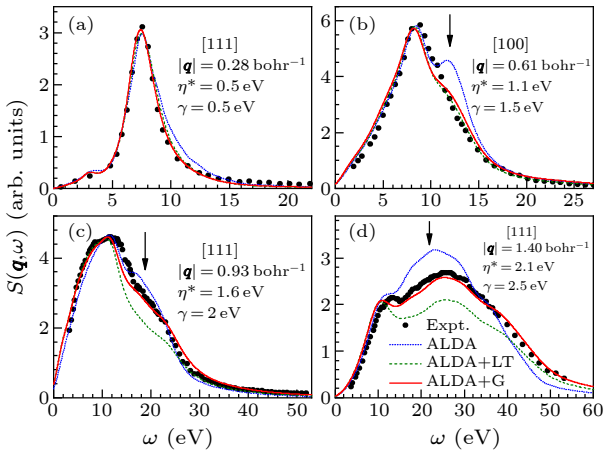

Fig. 1. Calculated DSF of Li together with IXS spectra measured by Schülke *et al.*[18,19] at selected $|\boldsymbol{q}|$ along [100] and [111] directions, where η^* is the broadening factor used in the TDDFT calculation with the ALDA kernel, and γ is the Gaussian broadening factor to account for the finite resolution in ω caused by the discrete sampling of the Brillouin zone.

However, when $|\boldsymbol{q}|$ further increases to far above $2q_c$, the lifetime broadening becomes insufficient to account for experimentally measured features. As shown in Figs. 1(c) and 1(d), the ALDA+LT results generally underestimate the strength of the spectra at high energy. However, the detailed features of the calculated spectrum, i.e., the fluctuations and ripples, are quite similar to those of the measured spectrum if the strength underestimation are not considered, see, e.g., the second peak indicated by the arrows in Figs. 1(c) and 1(d). It suggests that one may lift the ALDA+LT spectrum strength at high energy by introducing a scaling parameter in order to reproduce the experimental results. It turns out that the renormalization factor can serve the purpose in a simple way. It enters the ansatz as part of the screened Green's function G, as displayed in Eqs. (3) and (4), and the rescaling effect is presented by the combination of $|Z_k||Z_j|/\zeta$ in Eq. (4), which will be called the rescaling coefficient Γ hereafter. Figures 1(c) and 1(d) show that when Γ is included according to Eq. (4), the theoretical spectra are substantially improved and in close agreement with the experimental results up to $|\boldsymbol{q}| \approx 1.40$ bohr^{-1}, the highest transferred momentum measured for Li so far. DSFs of other transferred momenta and directions are provided in the Supplemental Materials,[66] showing a similar trend as that displayed in Fig. 1.

From the theoretical results in Fig. 1, one may have noticed that there is a hierarchy of approximations for the calculation of DSF with increasing sophistication and the application range of $|\boldsymbol{q}|$. It starts from the TDDFT method with an ALDA kernel, and then is improved by including lifetime broadening effects. A further improvement is achieved by taking into consideration of the rescaling effect of the renormalization factor, through the inclusion of the full screened Green's function. With the proposed ansatz, this hierarchy can be understood as a series of simplifications in the calculation of χ_0 in Eq. (4). The TDDFT method amounts to set the rescaling coefficient Γ to be 1 and to substitute the quasi-particle energies $\epsilon^{\rm QP}_{j,k}$ by the Kohn–Sham eigen-energies $\epsilon^{\rm KS}_{j,k}$. Note that, in practice, the TDDFT calculation is usually carried out with a small constant lifetime broadening.[67] Further including the lifetime broadening effect leads to the TDDFT method with lifetime correction proposed by Weissker *et al.*[16,46] When all the features of the screened Green's function are taken into consideration, the complete formula of the ansatz will be recovered.

In order to understand how the hierarchy of approximations works, we plot the quasi-particle properties, i.e., the rescaling coefficient Γ, the quasi-particle energy shift $\Delta = \Re(\epsilon^{\rm QP}_k - \epsilon^{\rm QP}_j) - (\epsilon^{\rm KS}_k - \epsilon^{\rm KS}_j)$, and the lifetime broadening $\eta = \Im(\epsilon^{\rm QP}_k - \epsilon^{\rm QP}_j)$ of electron-hole pairs in Fig. 2, with respect to the transition energy $(\epsilon^{\rm KS}_k - \epsilon^{\rm KS}_j)$ calculated using the DFT method. It shows that there is an abrupt change taking place at a transition energy around $2\omega_p$ for all of the three properties. Note that ω_p for Li is 7.12 eV.[68] Below the energy, which is about 15 eV for Li, Γ is roughly a constant about 1, the quasi-particle energy shift is close to zero, and the lifetime broadening increases monotonically from zero to about 1.4 eV. Above the energy, the rescaling coefficient is rapidly lifted to a value between 1.2 and 1.7, the quasi-particle energy shift starts to increase linearly, and the lifetime broadening jumps to a value in the range from 2.3 to 4.7 eV.

These features help to determine the validity regime of the series of approximations. For example, for the metallic Li, the main feature of the DSF spectrum at small $|\boldsymbol{q}|$ is a plasmon peak centered at around 7 eV with a full width of half maximum of about 3 eV, as displayed in Fig. 1(a).

In this limited energy range, the rescaling coefficient is around 1, the quasi-particle energy shift is close to zero, and the lifetime broadening is between 0.45 to 0.75 eV. When this energy-dependent lifetime broadening is approximated by a small constant broadening factor about 0.6 eV, the calculation is reduced to a TDDFT calculation in common practice.

However, when the spectrum covers a larger energy range, as it usually does when $|\boldsymbol{q}|$ increases, a constant lifetime broadening is not enough to account for the broadening of the spectrum for the entire energy range. In particular, when $|\boldsymbol{q}|$ increases to some magnitude such that the main feature of the spectrum is located in an energy range from 0 to about $2\omega_p$, i.e., about 15 eV for Li, it would be necessary to take the full energy-dependent lifetime broadening into consideration to arrive at a good approximation, i.e., the lifetime corrected TDDFT method proposed by Weissker *et al.* [16,25,35,46,47] is recovered, since in this energy range the rescaling coefficient is still around 1 and the quasi-particle energy shift is close to zero. This is exactly what Figs. 1(b) and 2 have illustrated, where the rescaling coefficient is about 1, and the quasi-particle energy shift is less than 0.5 eV.

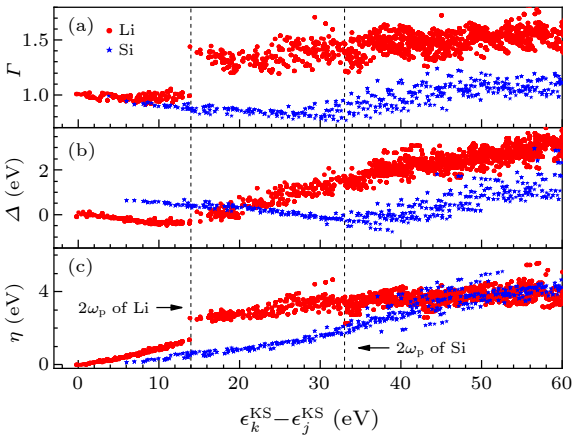

Fig. 2. The rescaling coefficient, quasi-particle energy shift, and lifetime broadening of Li and Si, calculated for electron-hole pairs of the GW method. (a) The rescaling coefficient Γ, defined as $\Gamma = |Z_k||Z_j|/\zeta$. (b) The quasi-particle energy shift Δ, defined as $\Delta = \Re(\epsilon_k^{\rm QP} - \epsilon_j^{\rm QP}) - (\epsilon_k^{\rm KS} - \epsilon_j^{\rm KS})$. (c) The lifetime broadening η, defined as $\eta = \Im(\epsilon_k^{\rm QP} - \epsilon_j^{\rm QP})$. Note that forbidden transitions are not presented in the figure.

Further increasing $|\boldsymbol{q}|$ makes the spectrum range go beyond the $2\omega_p$ threshold, as displayed in Figs. 1(c) and 1(d), it is then necessary to take into account the full feature of the screened Green's function. Figure 2 shows that in addition to the significant change of the quasi-particle energy shift and lifetime broadening, the rescaling coefficient also experiences an abrupt increase from 1 to a value between 1.2 and 1.7 when crossing the $2\omega_p$ threshold, as the result of a sharp increase of the renormalization factor $|Z|$ of quasi-electrons from 0.6 to a value between 0.8 and 1.0, [69] which is induced by the excitation of plasmon poles in the dynamical screening to Coulomb potential. [47,70,71] Under this condition, the complete form of the ansatz in Eq. (4), which includes the variation of renormalization factor, becomes indispensable for a satisfactory prediction of DSF spectra.

From Fig. 2, one can also see how the strength of the DSF is affected by the three quantities, i.e., the rescaling factor coefficient Γ, the quasi-particle energy shift Δ, and the lifetime broadening η. Since the major corrections are prominent for large transfer momentum $\boldsymbol{q}$, where χ can be well approximated by χ_0 according to Eq. (2), as can be seen if one notices that the kernel K decays to zero as q^{-2} at large $|\boldsymbol{q}|$ [1] in Eq. (2). Using the spectrum of Li in Fig. 1(d) as an example, ALDA results, which do not have any of the three corrections, overestimate the spectrum strength between $\sim$15 eV to $\sim$ 30 eV, when compared with experiments. The ALDA+LT results, which include the corrections of both quasi-particle energy shift Δ and lifetime broadening η, but without the correction of rescaling factor Γ, show that the two quantities provide a smooth effect to the DSF strength through the expression of χ_0 in Eq. (4), for energy greater than $\sim$12 eV.

On the one hand, the monotonically increasing Δ, which takes place from $\sim$12 eV for lithium, as displayed in Fig. 2(b), decreases the joint density of states, which is proportional to the strength of DSF. On the other hand, η provides an additional increase of the broadening effect, which further decreases the strength of the DSF. The overall effects of these two quantities, however, give rise to an overshoot, resulting in an underestimated DSF strength compared to the experiments. Figure 2(a) shows that the rescaling factor Γ increases from about 1 to 1.5, which gives a boost to the strength of the DSF to recover the experimental spectrum for energy greater than 12 eV.

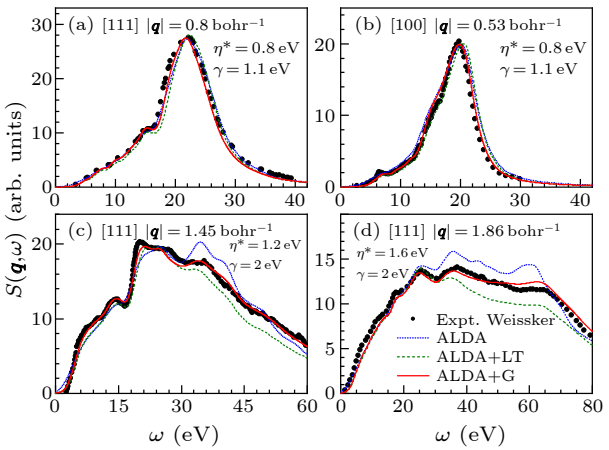

Fig. 3. Calculated DSF together with IXS spectra measured by Weissker *et al.* [16,46] at selected $|\boldsymbol{q}|$ from 0.53 bohr^{-1} to 1.86 bohr^{-1} along [100] and [111] directions. The ALDA results are calculated with a constant broadening η^* as indicated. Additional Gaussian broadening of width γ indicated is carried out at the end of each calculation to account for the finite resolution of ω.

The new method also applies to the DSF calculation of typical semiconductors. Its capability to provide much-improved predictions is displayed in Fig. 3 using Si as an

illustrating example. In order to reveal the contribution of the renormalization factor $|Z|$ (via the rescaling coefficient Γ) to the spectrum, results of the ALDA+LT method are also displayed together with the experimental measurements.[16,46] Figures 3(a) and 3(b) show that when the major feature of the spectrum is located below ~ 32 eV, the correction from the rescaling coefficient is small. However, when the spectrum feature goes beyond the energy, the rescaling coefficient contributes a significant increase in the spectrum strength compared to the ALDA+LT results, as shown in Figs. 3(c) and 3(d). It suggests that the improvement mainly comes from the subtle balance between the lifetime broadening and the rescaling of renormalization factors. A collection of the DSF of various directions and transferred momenta can be found in the Supplemental Materials.[72] In addition, one can also expect that the preceding arguments for the validity regime of approximations also apply to Si. As displayed in Fig. 2, the transition energy is around 32 eV, which is roughly twice the plasmon frequency of Si about 16.5 eV.[68]

In summary, we propose a composite ansatz without adjustable parameters to take the full feature of the screened Green's function, especially the renormalization factors, into consideration in the TDDFT calculation framework of the DSF. We show with Li and Si as illustrating examples that the proposed method provides a much-improved prediction to the DSF for typical metallic and semiconductor systems up to large $|\boldsymbol{q}|$. The new method may bring about interesting possibilities. For example, it may be used in experiments to directly infer the electronic structure from the DSF spectrum (with the help of statistical techniques such as the Bayesian inference method[73]), by taking the advantage of the relatively simple form of the ansatz and the much-improved theoretical results in a broad range of $\boldsymbol{q}$. The new method also forms an improved theoretical base for the diagnostics of temperature and density inside dense plasmas.

Acknowledgements. This work was supported by the National Natural Science Foundation of China (Grant Nos. 12375234, 12005012, and U1930402), and the Laboratory Youth Fund of Institute of Applied Physics and Computational Mathematics (Grant No. 6142A05QN21005).

References

[1] Onida G, Reining L, and Rubio A 2002 *Rev. Mod. Phys.* **74** 601
[2] Schülke W 2007 *Electron Dynamics by Inelastic X-Ray Scattering* (New York: Oxford University Press)
[3] Panholzer M, Gatti M, and Reining L 2018 *Phys. Rev. Lett.* **120** 166402
[4] Glenzer S H, Gregori G, Lee R W, Rogers F J, Pollaine S W, and Landen O L 2003 *Phys. Rev. Lett.* **90** 175002
[5] Glenzer S H and Redmer R 2009 *Rev. Mod. Phys.* **81** 1625
[6] Frydrych S, Vorberger J, Hartley N J *et al.* 2020 *Nat. Communications* **11** 2620
[7] Astapenko V A, Rosmej F B, and Khramov E S 2021 *Matter Radiat. At. Extremes* **6** 054404
[8] Li B, Ding Y, Kim D Y, Wang L, Weng T C, Yang W, Yu Z, Ji C, Wang J, Shu J, Chen J, Yang K, Xiao Y, Chow P, Shen G, Mao W L, and Mao H K 2021 *Phys. Rev. Lett.* **126** 036402
[9] Shen G Y and Mao H K 2017 *Rep. Prog. Phys.* **80** 016101
[10] Lee S K, Kim Y H, Yi Y S, Chow P, Xiao Y, Ji C, and Shen G 2019 *Phys. Rev. Lett.* **123** 235701
[11] Hagiya T, Matsuda K, Hiraoka N, Kajihara Y, Kimura K, and Inui M 2020 *Phys. Rev. B* **102** 054208
[12] Hill J P, Kao C C, Caliebe W A C, Gibbs D, and Hastings J B 1996 *Phys. Rev. Lett.* **77** 3665
[13] Reed J P, Uchoa B, Joe Y I, Gan Y, Casa D, Fradkin E, and Abbamonte P 2010 *Science* **330** 805
[14] Bradley J A, Seidler G T, Cooper G, Vos M, Hitchcock A P, Sorini A P, Schlimmer C, and Nagle K P 2010 *Phys. Rev. Lett.* **105** 053202
[15] Wang S X and Zhu L F 2020 *Matter Radiat. At. Extremes* **5** 054201
[16] Weissker H C, Serrano J, Huotari S, Bruneval F, Sottile F, Monaco G, Krisch M, Olevano V, and Reining L 2006 *Phys. Rev. Lett.* **97** 237602
[17] Eisenberger P, Platzman P M, and Schmidt P 1975 *Phys. Rev. Lett.* **34** 18
[18] Schülke W, Nagasawa H, and Mourikis S 1984 *Phys. Rev. Lett.* **52** 2065
[19] Schülke W, Nagasawa H, Mourikis S, and Lanzki P 1986 *Phys. Rev. B* **33** 6744
[20] Sturm K, Schülke W, and Schmitz J R 1992 *Phys. Rev. Lett.* **68** 228
[21] Egerton R F 2011 *Electron Energy-Loss Spectroscopy in the Electron Microscope* 3rd edn (New York: Springer Science & Business Media)
[22] de García A F J 2010 *Rev. Mod. Phys.* **82** 209
[23] Wu M, Shi R, Qi R, Li Y, Feng T, Liu B, Yan J, Li X, Liu Z, Wang T, Wei T, Liu Z, Du J, Chen J, and Gao P 2023 *Chin. Phys. Lett.* **40** 036801
[24] Hambach R, Giorgetti C, Hiraoka N, Cai Y Q, Sottile F, Marinopoulos A G, Bechstedt F, and Reining L 2008 *Phys. Rev. Lett.* **101** 266406
[25] Cazzaniga M, Weissker H C, Huotari S, Pylkkänen T, Salvestrini P, Monaco G, Onida G, and Reining L 2011 *Phys. Rev. B* **84** 075109
[26] Spence J C H and Spargo A E C 1971 *Phys. Rev. Lett.* **26** 895
[27] Schattschneider P, Födermayr F, and Su D S 1987 *Phys. Rev. Lett.* **59** 724
[28] Sternemann C, Huotari S, Vankó G, Volmer M, Monaco G, Gusarov A, Lustfeld H, Sturm K, and Schülke W 2005 *Phys. Rev. Lett.* **95** 157401
[29] Huotari S, Sternemann C, Schülke W, Sturm K, Lustfeld H, Sternemann H, Volmer M, Gusarov A, Müller H, and Monaco G 2008 *Phys. Rev. B* **77** 195125
[30] Sternemann H, Soininen J A, Sternemann C, Hämäläinen K, and Tolan M 2007 *Phys. Rev. B* **75** 075118
[31] Sahle C J, Sternemann C, Schmidt C *et al.* 2013 *Proc. Natl. Acad. Sci.* **110** 6301
[32] Fister T T, Nagle K P, Vila F D, Seidler G T, Hamner C, Cross J O, and Rehr J J 2009 *Phys. Rev. B* **79** 174117
[33] Fister T T, Fong D D, Eastman J A, Iddir H, Zapol P, Fuoss P H, Balasubramanian M, Gordon R A, Balasubramaniam K R, and Salvador P A 2011 *Phys. Rev. Lett.* **106** 037401
[34] Fan X H, Xu B, Niu Z, Zhai T G, and Tian B 2012 *Chin. Phys. Lett.* **29** 048102
[35] Huotari S, Cazzaniga M, Weissker H C, Pylkkänen T, Müller H, Reining L, Onida G, and Monaco G 2011 *Phys. Rev. B* **84** 075108
[36] Abbamonte P, Graber T, Reed J P, Smadici S, Yeh C L, Shukla A, Rueff J P, and Ku W 2008 *Proc. Natl. Acad. Sci.* **105** 12159
[37] Sundermann M, van der Laan G, Severing A, Simonelli L, Lander G H, Haverkort M W, and Caciuffo R 2018 *Phys. Rev. B* **98** 205108

[38] Sperling P, Gamboa E J, Lee H J, Chung H K, Galtier E, Omarbakiyeva Y, Reinholz H, Röpke G, Zastrau U, Hastings J, Fletcher L B, and Glenzer S H 2015 *Phys. Rev. Lett.* **115** 115001

[39] Mo C J, Fu Z G, Kang W, Zhang P, and He X T 2018 *Phys. Rev. Lett.* **120** 205002

[40] Mo C J, Fu Z G, Zhang P, Kang W, Zhang W, and He X T 2020 *Phys. Rev. B* **102** 195127

[41] Falk K, Holec M, Fontes C J, Fryer C L, Greeff C W, Johns H M, Montgomery D S, Schmidt D W, and Šmíd M 2018 *Phys. Rev. Lett.* **120** 025002

[42] Dornheim T, Böhme M, Kraus D, Döppner T, Preston T R, Moldabekov Z A, and Vorberger J 2022 *Nat. Commun.* **13** 7911

[43] Runge E and Gross E K U 1984 *Phys. Rev. Lett.* **52** 997

[44] Petersilka M, Gossmann U J, and Gross E K U 1996 *Phys. Rev. Lett.* **76** 1212

[45] Han J S, Lai K, Yu X X, Chen J H, Guo H L, and Dai J Y 2023 *Chin. Phys. Lett.* **40** 067801

[46] Weissker H C, Serrano J, Huotari S, Luppi E, Cazzaniga M, Bruneval F, Sottile F, Monaco G, Olevano V, and Reining L 2010 *Phys. Rev. B* **81** 085104

[47] Seidu A, Marini A, and Gatti M 2018 *Phys. Rev. B* **97** 125144

[48] Ding Y, Brachmann A, Decker F J, Dowell D, Emma P, Frisch J, Gilevich S, Hays G, Hering P, Huang Z, Iverson R, Loos H, Miahnahri A, Nuhn H D, Ratner D, Turner J, Welch J, Hering P, and Wu J 2009 *Phys. Rev. Lett.* **102** 254801

[49] Wu J L, Qi R Z, Huang Q S, Feng Y F, Wang Z S, and Xin Z H 2019 *Chin. Phys. Lett.* **36** 120701

[50] Hedin L 1965 *Phys. Rev.* **139** A796

[51] Hybertsen M S and Louie S G 1986 *Phys. Rev. B* **34** 5390

[52] Northrup J E, Hybertsen M S, and Louie S G 1987 *Phys. Rev. Lett.* **59** 819

[53] Pines D and Noziéres P 1966 *The Theory of Quantum Liquids* (New York: Benjamin) vol 1

[54] Mahan G D 2000 *Many-Particle Physics* 3rd edn (New York: Springer Science & Business Media)

[55] Yi Z J 2015 *Chin. Phys. Lett.* **32** 017101

[56] Frank W, Breier U, Elsässer C, and Fähnle M 1996 *Phys. Rev. Lett.* **77** 518

[57] Touloukian Y S 1975 *Thermal Expansion: Metallic Elements and Alloys* (New York: IFI/Plenum)

[58] Li H 1980 *J. Phys. Chem. Ref. Data* **9** 561

[59] Ashcroft N W and Mermin N D 1976 *Solid State Physics* (New York: Holt, Rinehart and Winston)

[60] Giannozzi P, Baroni S, Bonini N *et al.* 2009 *J. Phys.: Condens. Matter* **21** 395502

[61] Giannozzi P, Andreussi O, Brumme T *et al.* 2017 *J. Phys.: Condens. Matter* **29** 465901

[62] Monkhorst H J and Pack J D 1976 *Phys. Rev. B* **13** 5188

[63] Marini A, Hogan C, Grüning M, and Varsano D 2009 *Comput. Phys. Commun.* **180** 1392

[64] Sangalli D, Ferretti A, Miranda H, Attaccalite C, Marri I, Cannuccia E, Melo P, Marsili M, Paleari F, and Marrazzo A 2019 *J. Phys.: Condens. Matter* **31** 325902

[65] Gross E K U and Kohn W 1985 *Phys. Rev. Lett.* **55** 2850

[66] See the Supplemental Materials for other transferred momenta and directions of Li in Section I.

[67] Timrov I, Vast N, Gebauer R, and Baroni S 2013 *Phys. Rev. B* **88** 064301

[68] Kittel C 2018 *Introduction to Solid State Physics* (Singapore: John Wiley & Sons)

[69] The modulus of renormalization factor Z and other quasiparticle properties can be found in the Supplemental Materials.

[70] Shung K W K, Sernelius B E, and Mahan G D 1987 *Phys. Rev. B* **36** 4499(R)

[71] Quinn J J 1962 *Phys. Rev.* **126** 1453

[72] See the Supplemental Materials for DSF about other transferred momenta and directions of Si

[73] Lindley D V 1972 *Bayesian Statistics: A Review* (Philadelphia: Society for Industrial and Applied Mathematics)